JTTEE 2:257-264

Study of Fracture and Erosive Wear of Plasma Sprayed Coatings

D.Z. Guo and L.J. Wang

Double cantilever beam (DCB) and short bar (SB) specimens were used to determine the critical strain energy release rate (G_{IC}) of plasma-sprayed coatings of ZrO_2-base ceramic and WC-Co coatings. Erosion rates were measured for various erosive conditions. By comparing the G_{Ic} data and erosion rate (E_v) data with X-ray diffraction and fractographic analysis, fracture and erosion mechanisms of plasma-sprayed coatings were proposed. Based on the erosion models for brittle materials, a proportional relationship between the erosion rate, E_v, and G_{IC} was derived as follows:

$$E_v \propto \left(\frac{1}{H}\right)^{1/4} \times (G_{IC})^{-2/3}$$

where H is hardness. An increase in G_{IC} leads to a decrease in E_v. The exponent value of –2/3 of G_{IC} was confirmed by the experimental data.

1. Introduction

PLASMA spraying has been widely used in many branches of industry such as aviation, aerospace, energy and chemical engineering, etc.,[1-4] to improve surface properties and to prevent premature failure of components. The surface coatings of components in gas turbines, missile propellers, and fluidized beds are subjected to erosive wear by impingement of solid particles as well as elevated temperature corrosion. Sometimes, erosive wear is the decisive factor that limits the development of other material properties. Hence, research on coating erosive wear has practical significance.

In evaluating mechanical properties, fracture mechanisms, and related factors for coatings, the fracture mechanics method is superior to the conventional tension adhesion tests (TAT) in terms of distinguishing physical characteristics. McPherson et al.[1,2,5,6] chose the double cantilever beam (DCB) method to measure the critical strain energy release rate[7,8] of thermal sprayed coatings.

Evans correlated erosive wear of brittle materials to the fracture toughness of the bulk ceramics.[9,10] Levy[3,4,11,12] conducted tests on the erosive wear of thermal sprayed coatings, mainly with respect to intrinsic factors such as the fineness of powders, porosity, hardness, bonding force, and extrinsic factors such as erodent and environment. The above work did not address the relationship of fracture toughness and erosive wear resistance of coatings, modeling of fracture mechanisms, and mathematical expressions in detail.

It is assumed that the fracture mechanics method can be applied to describe the erosive wear resistance of coatings, because these coatings are usually more brittle than their corresponding bulk materials. In the present study, ZrO_2-based ceramic and WC-Co cermets were used as coating materials. The double cantilever beam and short bar (SB) methods were chosen to determine the critical strain energy release rate, G_{IC}. The SB method was first introduced to determine G_{IC}. The erosive wear test was conducted in a customized erosive wear machine. The erosive wear process, fracture of coatings, and the qualitative correlation of fracture toughness with erosive wear are discussed in this article.

Key Words: erosive wear, fracture models, fracture toughness, mechanical testing, tungsten carbide-cobalt, zirconia-yttria

D.Z. Guo and **L.J. Wang,** Department of Materials Engineering, Xian Jiaotong University, Xi'an, China.

2. Experimental Procedure

2.1 *Coating Materials*

Four materials were adopted for the research (Table 1). The processing procedures followed the manufacturers' recommended plasma spraying parameters.

2.2 *Erosive Wear Test*

The principle of the customized CMS-100 erosive wear machine is based on a vacuum chamber and free-falling abrasive materials that impinge on four rapidly rotating samples fixed on a rotating wheel. The vacuum eliminates the mechanical effects of air on impact velocity and impact angle.[13] The erosive wear panels (0.45% carbon plain-carbon steel) were 25 × 10 mm and 5 mm thick. The thickness of coatings, δ, was held at 0.2 to 0.3 mm. The noncoated faces of the samples were shielded with 0.05 mm thick copper foil.

The abrasive material was 80 to 100 mesh quartz sand of 0.15 to 0.2 mm diameter, and with a hardness of 1050 to 1160 HV. The erosive impact velocities, V_E, were 30, 50, and 70 m/s. The impact angles of 30° and 90° were chosen to contrast material properties of toughness and brittleness under erosive wear conditions. Test specimens were rinsed in alcohol and acetone and then dried. Weight loss was measured to 1×10^{-4} g sensitivity. The steady erosive wear rates of coatings were calculated by the following expressions. The weight of erosive wear rate, E_W, is

Table 1 Properties of plasma-sprayed coatings

Powders	Contents, wt%	Hardness, HRC	Density	Powder size
ZrO_2-5CaO	5% CaO, bal ZrO_2	32-45	5.20	−140 mesh + 10 μm
ZrO_2-8Y_2O_3	8% Y_2O_3, bal ZrO_2	35-45	5.10	...
WC-12Co (Metco 71VF-NS)	12% Co, bal WC	58	13.80	−45 + 5 μm
WC-17Co (Metco 73F-NS-1)	17% Co, bal WC	55	12.20	−53 + 10 μm

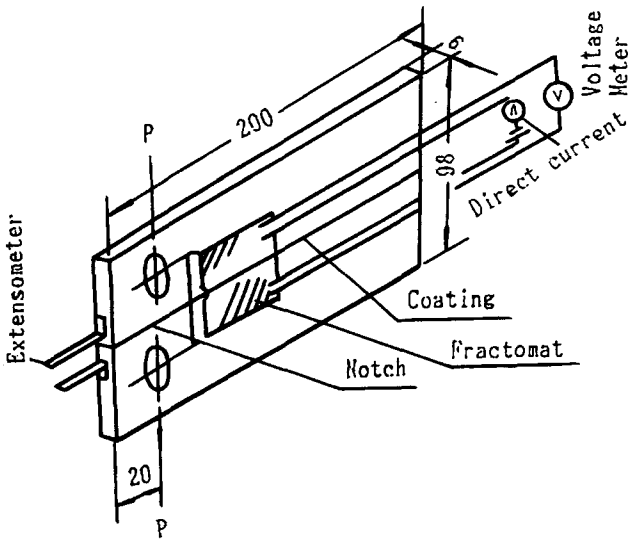

Fig. 1 Specimen geometry and extensometer placement for the double cantilever beam (DCB) method of finding coating fracture toughness.

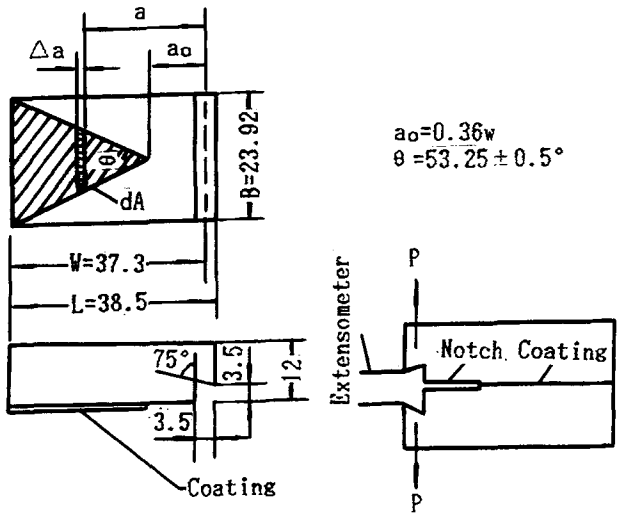

Fig. 2 Specimen geometry and extensometer placement for the short bar (SB) method of finding coating fracture toughness.

$$E_W = \frac{\Delta Wt}{We} \text{ (g/g)} \quad [1]$$

where ΔWt is the weight loss of the coating, and We is the weight of the erosive particle. The volume of erosive wear rate, E_v, is

$$E_v = \frac{E_W}{\rho} (mm^3/g) \quad [2]$$

where ρ is the density of the coating material.

2.3 *Measurement of Critical Strain Energy Release Rate*

2.3.1 Specimen Preparation

The G_{IC} of the coatings was measured using the DCB specimen shown in Fig. 1 and the SB specimen shown in Fig. 2. Both types of specimens were made by putting a hotset epoxy resin film between the coated and uncoated matching surfaces of two halves of the specimen, tightening the two halves firmly, and then holding the specimen in an oven at 180 °C for 3 h. The notch for the specimen was cut before the gluing procedure. The coating thickness should be greater than the penetration thickness of the glue and usually a coating thickness greater than 0.25 mm was required.

The test was considered invalid if crack growth occurred in the mixed lamellae of the glue and coating. The types of fracture can be divided into three groups—cohesive fracture (C type) where the crack grows inside of the coating lamellae, adhesive fracture (A type) where the crack grows along the interface between the coating and the substrate, and mixed fracture (A + C type) where both of the above fractures coexist.

2.3.2 Double Cantilever Beam Method

According to linear elastic fracture mechanics (LEFM), G_{IC} can be obtained by the compliance calibration:

$$G_I = \frac{P^2}{2B}\frac{dC}{da} \quad [3]$$

where G_I is the strain energy release rate of crack propagation; P is the imposed load on the specimen; C is the specimen compliance along the loading line; a is the length of the crack; and B is the thickness of the specimen. The tests were carried out on an Instron 1195 tensile machine at a loading rate of 0.05 mm/min. Unloading was performed when the load displacement ($P - \Delta$) curve deviated from a straight line. Figure 3 shows a series of $P - \Delta$ curves. The calibration procedures are described below.

Three uncoated glued samples were taken as calibrating samples because of the minor difference in dC/da calibration for coated and uncoated specimens.[1] TS-A20 fractomats were glued on the surfaces along the gluing direction. A three-pen X-Y recorder was used to simultaneously record the $P - \Delta$ curve and voltage variation-displacement ($\Delta V - V$) curve of the fractomat.[14] The compliance, C, at crack length, a, is equal to the reciprocal of the slope in unloading the straight line portion of the

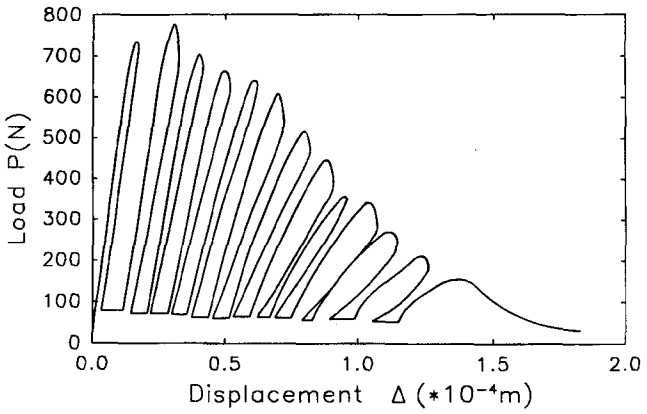

Fig. 3 Multiple deflection versus load (Δ versus P) data established from the DCB method.

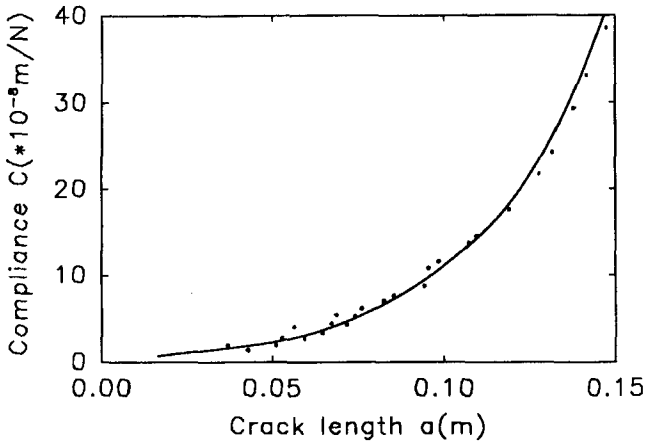

Fig. 4 Crack length versus compliance (a versus C) calibration curve for the DCB method.

previous $P - \Delta$ curve. A series of C versus a data was thus obtained. Figure 4 shows the regression lines for the data:

$$C(a) = \frac{0.6(a - 0.02)}{a} \exp(28.759\, a) \quad [4]$$

$$\frac{dC}{da} = 0.6 \exp(28.759\, a)\left(\frac{28.759\, a^2 - 0.575\, a + 0.02}{a^2}\right) \quad [5]$$

The correlation coefficient was 0.989. The calculation method for G_{IC} is as follows. The compliance corresponding to the unloading portion of each $P - \Delta$ curve was taken from the $P - \Delta$ curves in Fig. 3. The value of a was obtained from Eq 4. G_{IC} was then calculated using Eq 5 to find dC/da and hence applying Eq 3.

2.3.3 Short Bar Method

According to the compliance calibration method of fracture mechanics, G_{IC} can be given by:

$$G_1 = \frac{P^2}{W} Y(\alpha) \quad [6]$$

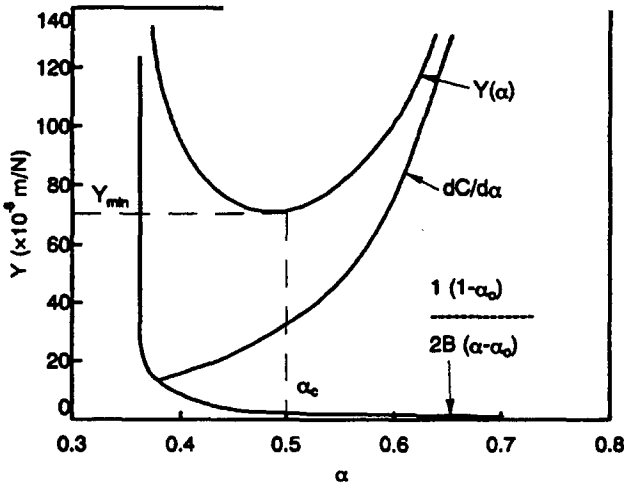

Fig. 5 Geometrical factor versus normalized crack length (Y-α) calibration curves for the SB method. The parameter α is dimensionless.

where

$$Y(\alpha) = \frac{1}{2B}\left(\frac{1-\alpha_o}{\alpha-\alpha_o}\right)\frac{dC}{d\alpha} \quad \alpha_o = \frac{a_o}{W} \quad \alpha = \frac{a}{W}$$

where C is the compliance of the specimen along the loading line; B, α_o, a, and W are shown in Fig. 2.

There exists a Y_{min} for the $Y(\alpha)$ versus α curve shown in Fig. 5. Y_{min} can be obtained by letting $dY/d\alpha = 0$, based on the Y versus α curve obtained from the specimens with $\alpha = 0.4$ to 0.85. The result is $Y_{min} = 87.478^{-6}$ m/N. Therefore, G_{IC} can be calculated from $G_{IC} = P_m^2 Y_{min}/W$, when Y_{min} and the maximum load, P_m, are known.

2.4 *Microscopic Analysis*

The fracture surface and erosive wear surface were examined using a JSM-35C Scanning Electron Microscope. A D/max-3a X-ray diffractometer was used to determine whether partially stabilized ZrO_2 exhibits phase transformation during the fracture and erosion processes. Following Evans, the fraction of monoclinic ZrO_2 can be evaluated by:

$$Fm = \frac{I_{M(111)}}{I_{T(111)} + I_{M(111)}} \quad [7]$$

where Fm is the fraction of the monoclinic phase (M); and $I_{M(111)}$ and $I_{T(111)}$ are the diffraction intensities of (111) plane of the M and T phases, respectively.

3. Results

Experimental data are shown in Table 2 for various erosive conditions. Each data point represents an average value of three points each from at least two specimens. The values of fracture toughness are given in Table 3, where G_{IC} is the average value

Table 2 Erosion test results of various coatings

V_E	30 m/s				50 m/s				70 m/s			
a_E	30		90°		30		90°		30		90°	
	E_W	E_V	E_W	E_V	E_W	E_V	E_W	E_V	E_W	E_V	E_W	E_V
ZrO_2-5CaO....	2.80	5.41	7.66	14.80	5.56	10.74	15.08	29.13	...	...	...	...
ZrO_2-8Y_2O_3 ..	6.35	12.45	14.13	27.80	19.30	37.84	39.65	77.75	44.3	86.86	...	...
WC-12Co	0.01	0.47	1.02	0.70	0.70	0.54	2.01	1.56	1.59	1.23	4.23	3.28
WC-17Co	0.87	0.71	1.23	1.00	1.80	1.46	2.32	1.89	2.44	1.98	4.69	3.81

Note: $E_W \times 10^{-4}$ g/g. $E_V \times 10^{-2}$mm^3/g.

Table 3 Critical strain energy release rate (G_{IC}), in J/m^2

		ZrO_2-5CaO		ZrO_2-8Y_2O_3	WC-12Co	WC-17Co	
	G_{IC}	124.17	62.45	31.98	604.09	404.32	205.25
SB	Fracture mode(a)	C	A	A	C	C	A
	ΔG_{IC}	13.2	10.2	15.8	153.5	46.6	49.8
	G_{IC}	40.7		32.5	...	...	
DCB	Fracture mode(a)	A		A	...	...	
	ΔG_{IC}	19.1		11.0	...	...	

(a) C refers to cohesive mode; A refers to adhesive mode.

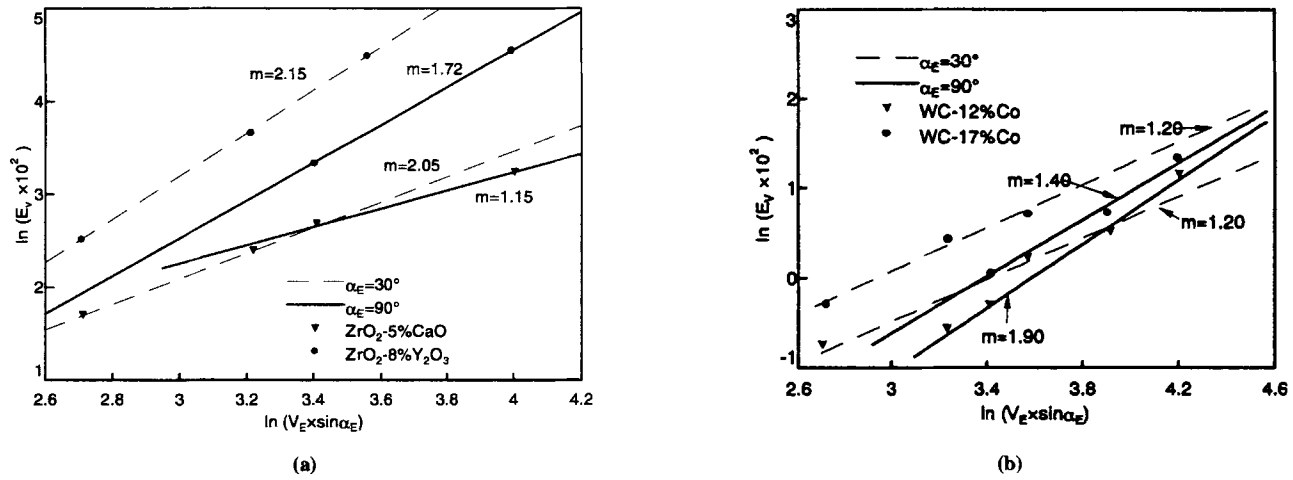

Fig. 6 Relation of vertical impact velocity versus erosion rate (ln { $V_E \times \sin[\alpha_E]$} versus ln{$E_V$}) for (a) zirconia and (b) tungsten carbide-cobalt coatings.

for each coating and ΔG_{IC} is the distribution deviation. The fracture mode is also presented. Each data point for the short bar method is the mean value of 4 to 6 specimens, whereas the data points for the DCB methods are the mean values of 20 to 30 data readings from three specimens.

The following relationships can be concluded from Tables 2 and 3. The G_{IC} and the erosion resistance of the ZrO_2 coating at various erosive conditions are lower than those of the WC-Co coating. The magnitude sequence of G_{IC} coincides with that of the erosion resistance in the order of the four types of coatings; i.e., WC-12Co, WC-17Co, ZrO_2-5CaO, and ZrO_2-8Y_2O_3. This trend qualitatively indicates that increasing the fracture toughness of the coating is beneficial to increasing its erosion resistance.

The erosion rate at the erosion angle $\alpha_E = 90°$ is higher than that at $\alpha_E = 30°$. It therefore behaves in a brittle manner and agrees with existing results for plasma-sprayed coatings.[3,4,11,12,15] The macrofractography of SB and DCB specimens also exhibited a brittle nature.

Using the vertical impact velocity ($V_E\perp = V_E \sin a_E$) to characterize the influence of impact velocity on the erosion rate of coatings, the $\ln E_v - \ln V_E\perp$ curves at various a_E are presented in Fig. 6. The linear relation obtained is consistent with the behavior of the bulk ceramic materials, where m is a constant and is referred to as the velocity exponent. The magnitude of m reflects the velocity sensitivity of the coatings for erosive wear. The general trend is that the lower the G_{IC} value, then the higher the m value.

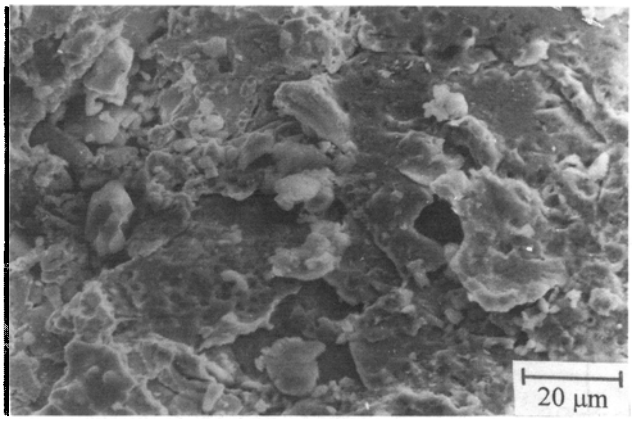

Fig. 7 Cohesive mode of fracture for WC-12Co coatings.

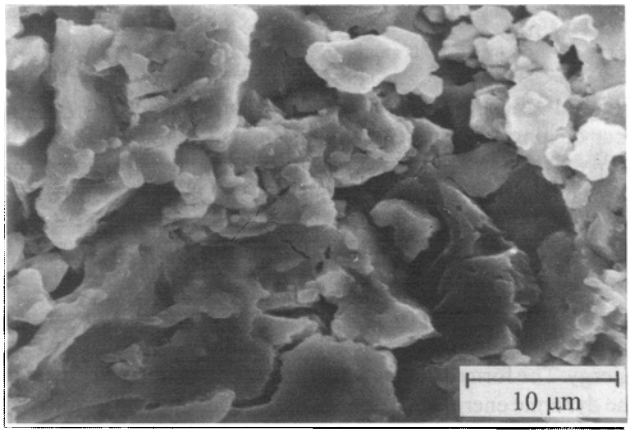

Fig. 8 Cohesive mode of fracture for ZrO_2-5CaO coatings.

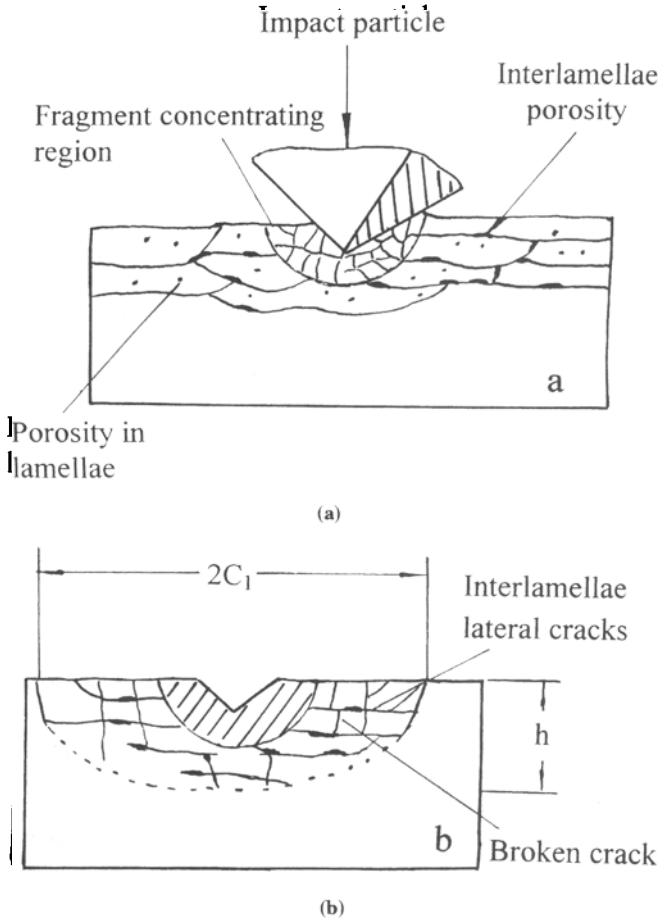

Fig. 9 Schematic of coating erosion. (a) Initial impact of the particle against the substrate and the so-formed crack features. (b) Coating removal and cracking that results in erosion.

Very similar results for G_{IC} were obtained by both the DCB and SB methods. The dominant fracture mode of the DCB specimen was adhesive for ZrO_2-based materials, but mixed modes were also present. For SB specimens of ZrO_2-5CaO and WC-17Co, the adhesive and cohesive fracture modes appear. The G_{IC} of the cohesive mode is almost twice that of the adhesive mode. This is similar to the results reported in Ref 5 and 6.

4. Discussion

4.1 *Test Method of G_{IC} for Coatings and Fracture Features*

Many theoretical and practical problems in the fracture mechanics measurement of coatings remain to be solved. For the determination of G_{IC}, the DCB and SB methods have their own merits. The former can provide several G_{IC} values from a single specimen, and one can obtain a statistical evaluation of reliability of coatings, but the experimental technique is more difficult and has many factors that can cause error. With the latter, one specimen provides one G_{IC} value, and the scatter of data is rather narrow. The experiment and calculation is simple and straightforward if Y_{min} has been calibrated. In this author's opinion, the better way is to combine the above two methods for directing coating design and processing technique optimization.

The same fracture mode in both methods of G_{IC} determination was confirmed by identical microcharacteristics. Figures 7 and 8 exhibit the cohesive type of fracture for WC-12Co and ZrO_2-5CaO coatings. The void pitting at the lamellae interfaces and the fracture interfaces can be distinguished. This is attributed to the concentration of voids at the interfaces of lamellae. No plastic deformation was observed, and this implies that cracks propagate along the lamellae boundaries of the coating where the crack growth resistance is low. There also appears to be some steps due to lamella fracture (Fig. 7 and 8). Thus, the main fracture mechanism of the coating is brittle fracture and validates G_{IC} measurements using LEFM.

4.2 *Surface Features of Eroded Coatings*

The erosion rate of WC-Co and ZrO_2-base coatings is higher than that of their corresponding bulk materials and is caused by the presence of lamellae and voids in the coatings which may break apart and crack. These features are more distinct for the ZrO_2-8Y_2O_3 material. Even at a low erosion angle ($a_E = 30°$), no plastic erosion features such as ploughing were observed,

and it is evident that brittle fracture dominates the fracture process. Figure 9 schematically illustrates the erosion process of a brittle, porous ceramic coating. Solid particles impinge on the coated surface and produce compressive stress, brittle fragmentation of lamellae, and densification of porosity. During particle impact, the fragment concentrated region is formed.

Figure 9(a) exhibits similar effects on the surrounding material as the indentation method of fracture toughness measurement. The impact energy of particles is converted to the energy needed for lateral and radial crack propagation in the surrounding material. The lateral cracks prefer to initiate along the lamellae boundaries where more voids exist. The intersection of lateral cracks with radial cracks leads to the removal of the material, as shown in Fig. 9(b). From this point of view, the erosion of the coating is a successive process consisting of a series of material removed by brittle fracture. Hence, erosion resistance can be physically related to the fracture toughness of the material.

4.3 *Relationship of Erosion Rate (E_V) to Fracture Toughness (G_{IC})*

Assuming that an erosion pit due to particle impact has a hemispherical shape (Fig. 9b), then its volume is proportional to:

$$E_V \propto C_1^2 \cdot h \quad [8]$$

where C_1 and h are the lateral crack length and depth at a given erosion condition, respectively. The lateral crack length, C_1, is proportional to the radial crack size, Cr.[9,10] Thus:

$$E_V \propto Cr^2 \cdot h \quad [9]$$

Referring to Evan's theory for bulk ceramics,[9,10] where h and target material hardness H could be related as:

$$h^2 \propto (1/H)^{1/2} \quad [10]$$

The driving force for crack extension during projectile impact is the dynamic tensile stress field, and the resistance to crack propagation is determined by the fractural toughness of the material. Evans[10] suggested that the correlation of radial crack size, Cr, with fracture toughness, K_{IC}, of a material can be given by:

$$Cr \propto K_{IC}^{-2/3} \quad [11]$$

and

$$K_{IC} \propto \left(G_{IC}\right)^{1/2} \quad [12]$$

also

$$Cr \propto \left(G_{IC}\right)^{-1/3} \quad [13]$$

Substitution of Eq 10 and 13 into Eq 9 gives:

$$E_V \propto (1/H)^{1/4} \cdot (G_{IC})^{-2/3} \quad [14]$$

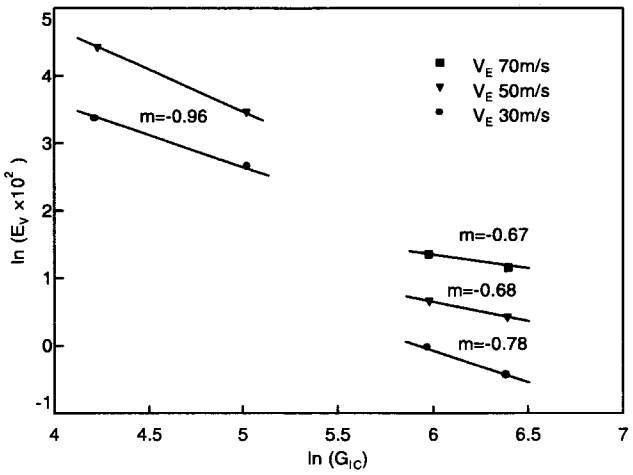

Fig. 10 Relationship of fracture toughness versus erosion rate (E_V versus G_{IC}).

Figure 10 illustrates the relationship of $\ln E_V$ versus $\ln G_{IC}$ for the four coatings. E_V and G_{IC} exhibit an exponential relation. The slopes of the straight lines (m) are about –2/3 and indicate that these experiments fit, reasonably well, the above assumed derivation.

Increasing G_{IC} leads to an increase in the erosion resistance of the coatings. This can be further explained in terms of energy consumption. Both processes of fracture and erosion include crack propagation along lamellae boundaries, and both expend energy. The former comes from extrinsic loading; the latter from the dynamic energy of the particles. The coating with higher G_{IC} has (1) higher energy needed for crack initiation and propagation, (2) better energy transfer to the surrounding lamellae and substrate, and (3) secondary crack formation (for WC-Co coatings) which consumes energy. These three aspects of the energy balance within the coating enhance the erosion resistance.

4.4 *Factors Influencing G_{IC} and E_V of Coatings*

Fine lamellae, low porosity, and high toughness are beneficial for increasing the G_{IC} and erosion resistance of a coating. The WC-Co coatings are superior to ZrO_2-base coatings. This is attributed to the following factors: finer powders, higher density, addition of Co as the adhering agent, and higher toughness of the lamellae. X-ray diffraction analysis indicates that the tetragonal phase transformation in two types of ZrO_2-base coatings is less than that in the bulk ZrO_2 ceramic. This occurs because cracks in coatings usually grow along lamellae boundaries, which need less energy and reduce tetragonal phase transformation.

5. Conclusions

Double cantilever beam and short bar methods can both be used to measure the G_{IC} of plasma-sprayed coatings. The WC-Co coatings exhibit a higher G_{IC} than ZrO_2-base coatings. The common fracture process in the four types of coatings is crack growth along interlamella boundaries. The thickness of lamellae

porosity, and toughness of lamellae affect the G_{IC} value. The WC-Co coatings are more erosion-resistant than ZrO_2-base coatings. This is consistent with the G_{IC} values. The erosion process in brittle coatings consists of the formation of fragmented regions by impact energy, the brittle deformation of surrounding lamellae, and the removal of fractured regions of lamellae due to lateral crack formation.

Based on the combination of fracture and erosion measurements for coatings, the relationship between E_V and G_{IC} can be formulated as:

$$E_V \propto \left(\frac{1}{H}\right)^{1/4} \cdot (G_{IC})^{-2/3}$$

E_V will therefore be decreased by increasing G_{IC}. The –2/3 exponent of the fracture toughness term was confirmed from these experiments.

References

1. P. Ostojic and R. McPherson, Determining the Critical Strain Energy Release Rate of Plasma-Sprayed Coating Using a Double-Cantilever-Beam Technique, *J. Ceram. Soc.*, Vol 71 (No. 10), 1988, p 891-899
2. R. McPherson, The Relationship Between the Mechanism of Formation, Microstructure and Properties of Plasma-Sprayed Coatings, *Thin Solid Films*, Vol 83, 1981, p 297-310
3. A.V. Levy and B. Wang, Erosion of Hard Material Coating Systems, *Wear*, Vol 121, 1988, p 325-346
4. A.V. Levy, The Erosion-Corrosion Behavior of Protective Coatings, *Surf. Coat. Technol.*, Vol 36, 1988, p 387-406
5. G.N. Heintze and R. McPherson, Fracture Toughness of Plasma-Sprayed Zirconia Coatings, *Surf. Coat. Technol.*, Vol 34, 1988, p 15-23
6. G.N. Heintze and R. McPherson, A Further Study of the Fracture Toughness of Plasma-Sprayed Zirconia Coatings, *Surf. Coat. Technol.*, Vol 36, 1988, p 125-132
7. A.G. Evans, M. Rühle, B.J. Dalgleish, and P.G. Charalambides, The Fracture Energy of Bimaterial Interfaces, *Mater. Sci. Eng.*, Vol A126, 1990, p 53-64
8. D.Z. Guo and L.J. Wang, Measurement of the Critical Strain Energy Release Rate of Plasma-Sprayed Coatings, *Surf. Coat. Technol.*, Vol 56, 1992, p 19-25
9. A.G. Evans, Impact Damage Mechanics Solid Projectiles, in *Treatise on Materials Science and Technology*, Vol 16, C.M. Preece, Ed., Academic Press, 1979, p 1-67
10. A.G. Evans, M.E. Gulden, and M. Rosenblatt, Impact Damage in Brittle Materials in the Elastic-Plastic Response Regime, *Proc. Roy. Soc. London*, Vol A361, 1978, p 343-365
11. A.V. Levy and G. Hickey, Erosion of Corrosion-Resistant Surface Treatments on Alloy Steels, *Wear Mater.*, 1985, p 699-707
12. A.V. Levy, D. Boone, A. Davis, and E. Scholz, The Erosion of Protective Coating, *Proc. 6th Int. Conf. Erosion by Liquid and Solid Impact*, Cambridge, Cambs., 5-8 Sept 1983, Cavendish Laboratory, Cambridge, Paper No. 46, 1983
13. S. Qisheng, CMS-100 Erosion Tester, *J. Xian. Jiaotong Univ.*, Vol 23 (No. 2), 1989, p 343-346 in Chinese
14. C. Yuhua, A New Technique for Measuring Fatigue Crack Growth, *J. Xian Jiaotong Univ.*, Vol 23 (No. 2), 1989, p 334-339 in Chinese
15. S. Srinivasan and R.O. Scattergood, Effect of Erodent Hardness on Erosion of Brittle Materials, *Wear*, Vol 128, 1988, p 139-152